Hindawi
Geofluids
Volume 2021, Article ID 6229095, 12 pages
https://doi.org/10.1155/2021/6229095

*Research Article*

# Particle Flow Analysis of Mechanical Properties and Failure Behaviour in Composite Rock Strata with Holes

**Chuanwei Zang**,[1] **Hongmo Zhu**,[1] **Miao Chen**,[1] **Shuo Yang**,[2] **Liu Yang**,[1] **Jia Zhou**,[1] **Zuoru Zhang**,[3] **and Yang Chen**[4]

[1]*College of Energy and Mining Engineering, Shandong University of Science and Technology, Qingdao, Shandong 266590, China*
[2]*School of Civil Engineering, Xuzhou University of Technology, Xuzhou, Jiangsu 221018, China*
[3]*The Green Aerotechnics Research Institute of Chongqing Jiaotong University, Chongqing 401120, China*
[4]*Key Laboratory of Urban Security and Disaster Engineering, Ministry of Education, Beijing University of Technology, Beijing 100124, China*

Correspondence should be addressed to Miao Chen; miaochen@sdust.edu.cn

Received 28 September 2021; Revised 17 November 2021; Accepted 24 November 2021; Published 14 December 2021

Academic Editor: Liang Xin



Understanding the deformation failure behavior of the composite rock strata has important implications for deep underground engineering construction. Based on the uniaxial compression laboratory test of the specimens of composite rock strata containing holes, the microscopic parameters in the particle discrete element simulation are firstly calibrated. Then, the mechanical properties and failure characteristics of the composite rock strata with holes under different confining pressures are studied. The results show that different dip angles and confining pressures have significant effects on the peak strength and elastic modulus of the specimens. Under the same confining pressure, the peak strength and elastic modulus decrease first and then increase with the increasing dip angle. As the dip angle is constant, both the peak strength and elastic modulus gradually increase with the increase in confining pressure. It shows that the first area to be damaged in composite rock strata transfers from soft rock to hard rock with the increase in dip angle. With the increase in confining pressure, the range of tensile stress concentration area decreases substantially, while the range of compressive stress concentration area changes less.

## 1. Introduction

With the advancement of underground engineering technology, more and more tunnels have been built in deep complex rock strata [1–3]. In the process of deep tunneling, alternating soft and hard composite rock strata are often encountered. The mechanical properties and failure behavior of composite rock strata were significantly different from those of homogeneous rocks. Therefore, the study of composite rock specimens containing holes has important engineering guidance significance for the safety and stability of rock engineering.

At the engineering scale, scholars have conducted various studies on tunneling in composite rock strata. Zhang et al. [4] conducted model tests of deeply buried tunnels in complex rock strata, the results showed that there are significant differences in the evolution and distribution characteristics of displacements and stresses in different rock formations. Huang et al. [5] carried out physical model tests to study the influence of weak interstates on the stability of the surrounding rock of the chamber. Wu et al. [6, 7] studied the characteristics of shotcrete and analyzed its influence on the stability of tunnel surrounding rock, and the method of yielding supports is proposed. Lin et al. [8] investigated the failure behavior of the tunnel of Jinping II Hydropower Station through geomechanical model tests, and the stress and displacement change rules under high ground stress are proposed. Liu et al. [9] conducted uniaxial compression tests on hard rock specimens containing elliptical holes and fissures, four failure modes of rock bridges have been

determined. Wu et al. [10] employed an improved creep mechanics model to predict the displacement of tunnel surrounding rock.

Scholars have also conducted in-depth studies on the mechanical properties and macroscopic failure behaviors of specimens containing holes at the laboratory scale. Si et al. [11] conducted a series of true triaxial tests with cubic specimens containing circular holes, and the results showed that the failure occurred first in the middle part on both sides of the hole, then developed rapidly to the deep part, and finally formed two symmetrical V-shaped cracks. Zhou et al. [12] conducted uniaxial compression tests on hard rock with four types of cavities, and the influence of the shape of the holes on the rock mechanical properties and the evolution of fracture failure are studied. Wu et al. [13] conducted a series of uniaxial compression tests using digital image techniques and acoustic emission to study the mechanical properties, failure characteristics and fracture features of the specimens with cross-excavation formed holes. Maji and Shah [14] carried out a series of uniaxial compression tests on concrete with two circular holes and prismatic concrete with fillings were tested in compression; finally, it was found that the cracking always starts at the interface of the fillings. Du et al. [15] performed uniaxial compression tests on hard rock and high-strength concrete with two holes, and then the final failure modes of all specimens are categorized as a tension-shear mixed failure and shear failure. Fakhimi et al. [16] conducted out biaxial compression tests on hard rocks containing prefabricated circular holes, and the acoustic emission characteristics during the failure process are investigated. The deformation and failure laws of jointed specimens with prefabricated circular holes under biaxial compression were studied by Sagonget.al [17]. Cheng et al. [18] investigated the influence of composite rock dip on the mechanical properties and macro failure mode of the specimen through compression test. Deng et al. [19] carried out the loading tests of sandstone with different bedding dip angles under uniaxial and triaxial conditions, the influence of bedding plane on the mechanical properties and failure mode of rock mass is researched.

Numerical simulation is an effective tool to study the excavation of underground rock mass engineering. Many scholars have obtained a large number of research results through numerical simulation. Feng et al. [20] used the finite difference software Fast Lagrangian Analysis of Continua in 3 Dimensions (FLAC3D) to analyze the evolution of principal stress when the Munigou tunnel crosses the soft and hard contact zone during excavation. They find that the local stress concentration effect controlled the large deformation of the soft rock in the tunnel. Yang et al. [21] simulated tunnel excavation and support in an inclined upper soft and lower hard rock strata with Universal Distinct Element Code (UDEC), and the change laws of surrounding rock stress and deformation are analyzed. Wang et al. [22] used Particle Flow Code in 2 Dimensions (PFC2D) to study the stress and displacement vector distribution characteristics of the composite specimens with holes and double cracks. The biaxial test was conducted on square specimens with a circular chamber with the Rock Failure Process Analysis (RFPA) software, and the failure process and influencing factors of this kind of rock were discussed by Zhu et.al [23]. Hou et al. [24, 25] investigated the effects of fracture complexity, air pressure, and other factors on shale gas flow; then, the failure law of tight rock specimens is obtained through numerical simulation. Liang [26] et al. proposed the initiation and expansion law of rock fissures under the action of water and nitrogen. Zhang et al. [27] discussed the stability control method of roadway driving near the working face, and the stress changes are obtained through numerical modeling.

Table 1: Physical and mechanical parameters of soft rock and hard rock.

| Lithology | $\sigma_c$ (MPa) | $\sigma_t$ (MPa) | $C$ (MPa) | $\Phi$ (°) | $E$ (GPa) | $\upsilon$ |
|---|---|---|---|---|---|---|
| Soft rock | 12.23 | 1.48 | 2.57 | 34 | 1.5 | 0.3 |
| Hard rock | 45.86 | 3.31 | 7.92 | 45 | 5.97 | 0.24 |

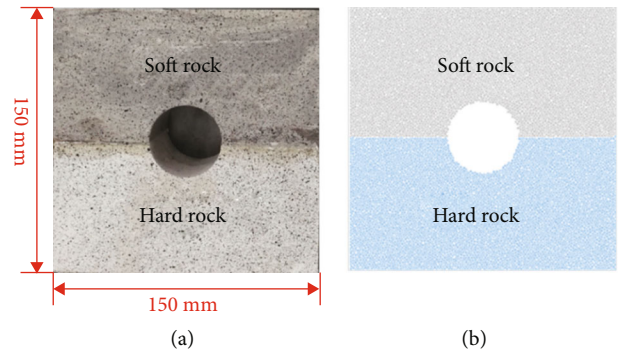


Figure 1: Schematic diagram of laboratory specimens and numerical simulation.

Although numerous previous studies have been conducted on chambers and tunnels under composite rock conditions, however, due to the complex occurrence of surrounding rocks during the excavation of underground engineering, the surrounding rocks of chambers and tunnels are often composed of rock strata with very different lithology. At the same time, due to the limitation of the laboratory test conditions, the previous research mostly focused on the uniaxial compression test, which is very different from the high confining pressure environment of the rock mass in deep engineering. In this paper, based on the uniaxial compression test of the composite rock strata with holes in the laboratory, the PFC2D software is used to conduct the biaxial compression test on the specimen of the composite rock strata with holes at different dip angles, and the influence of rock dip angle and confining pressure on the mechanical characteristics and failure modes of the specimen is studied.

## 2. Numerical Modeling Establishment

*2.1. Brief Introduction of the Laboratory Experiments.* The soft rock and hard rock materials are taken from Renshou County, Sichuan Province, and their mineral composition is mainly quartz and feldspar [28]. The physical and mechanical parameters of the rock specimen are shown in

Table 2: Microparameters used in PFC for complicated rock strata.

| | Effective modulus (GPa) | Bond effective modulus (GPa) | Cohesion (MPa) | Tensile strength (MPa) | Friction angle (°) | $\mu$ |
|---|---|---|---|---|---|---|
| Soft rock | 0.8 | 0.9 | 4.7 | 6.1 | 34 | 0.5 |
| Hard rock | 3 | 4.4 | 20.3 | 23.3 | 45 | 0.5 |
| Structural plane | 0.6 | 0.6 | 3 | 3.6 | 38 | 0.3 |

Table 1. The composite rock specimens were prepared by gluing the soft rock and hard rock, and the size of the square specimen was 150 mm × 150 mm × 45 mm. Then drill a hole in the center of the specimen with a diameter of 40 mm, and the final specimen is shown in Figure 1(a).

*2.2. Calibration of Microparameters in Numerical Modeling.* The numerical model established by PFC2D is a collection of rigid particles, which are bonded together by bonding. During the simulation, the motion of the particles follows Newton's second law of motion. Previous researches have shown that the parallel bonding model is more suitable for simulating rock-like materials [29], and the parallel bonding model is adopted in this simulation. The bond in the contact bonding model acts only on an infinitesimal contact point between two particles and can only transfer forces, while the bond in the parallel bonding model acts on a finite size circular cross section between two particles and can transfer both forces and moments [30, 31].Based on the laboratory test, the numerical model of 150 mm ×150 mm is established in PFC2D, as shown in Figure 1(b). The uniaxial compression specimen model was first established, and the microscopic parameters of soft rock and hard rock are calibrated by the "trial and error" method based on the uniaxial compression test data in Table 1. The final microscopic parameters obtained are shown in Table 2.

## 3. Simulation Results under the Uniaxial Compression

The stress-strain curves of the composite rock specimens containing holes at different angles ($\alpha = 0^\circ$, $30^\circ$, $60^\circ$, and $90^\circ$) from the numerical simulations are given in Figure 2. It can be known from Figure 2 that the curve of the stress-strain curve obtained by the PFC2D simulation does not have an initial compaction stage. This is due to the contact between particles in the numerical model being relatively uniform and dense, and there will be no closure of microcracks or defects during the load. The comparison of peak strength and elastic modulus of composite rock specimens with different rock angles under uniaxial compression in laboratory tests and PFC2D simulations is given in Figure 3. It is revealed that both the peak strength and the modulus obtained by experiment and simulation decreases first and then increases with the increase of the dip angle of the rock strata, and the difference between them is small.

The final failure mode simulation results of the composite rock specimens containing holes at different dip angles are compared with the laboratory test results in Figure 4.

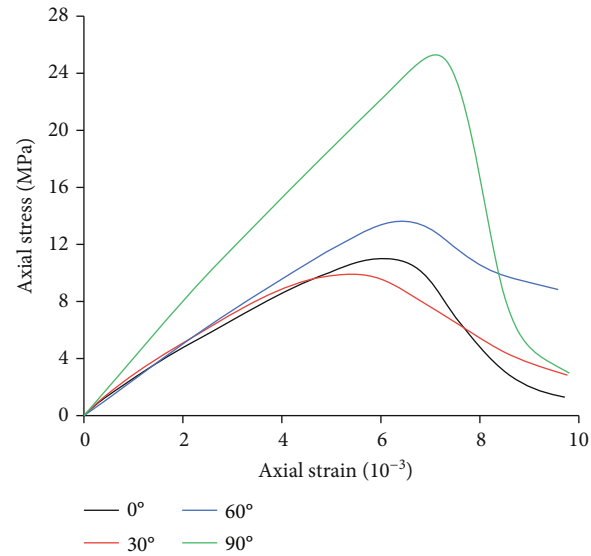


Figure 2: Simulated stress-strain curves under uniaxial compression.

When the dip angle of the specimen is 0°, a large number of microcracks are generated in the soft rock area. The failure degree of the soft rock area is greater than that of the hard rock area, forming a V-shaped fracture zone. As the dip angle increased to 30°, a large number of microcracks were generated along the structural plane near the soft rock side, the entire composite rock specimen is damaged by shear slip along the structural plane. When the dip angle of the specimen increases to 60°, the microcracks in the soft rock area on the right side of the hole continue to gather, connect, and penetrate to form a macroscopic fracture zone, and the hard rock area on the left side forms a shear fracture zone that penetrates the specimen. Analyzing the simulation diagram of the final failure of the specimen with a 90° dip angle, it can be seen that a large number of microcracks have occurred in the soft rock area and the hard rock area, forming an X-shaped shear fracture zone. By comparing, the simulation results of the specimens are consistent with the laboratory test results, indicating that the calibrated microscopic parameters are reasonable to simulate the composite rock specimens with holes.

## 4. Simulation Results under Biaxial Compression

*4.1. Analysis of Mechanical Properties under the Biaxial Test.* To study the failure characteristics of composite rock

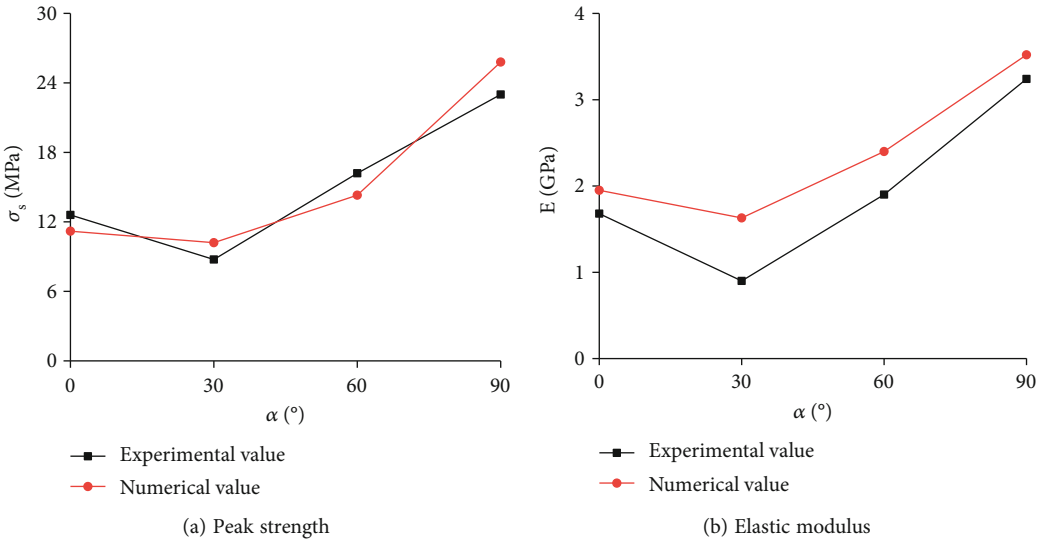


Figure 3: Comparison between the numerical results and experimental results.

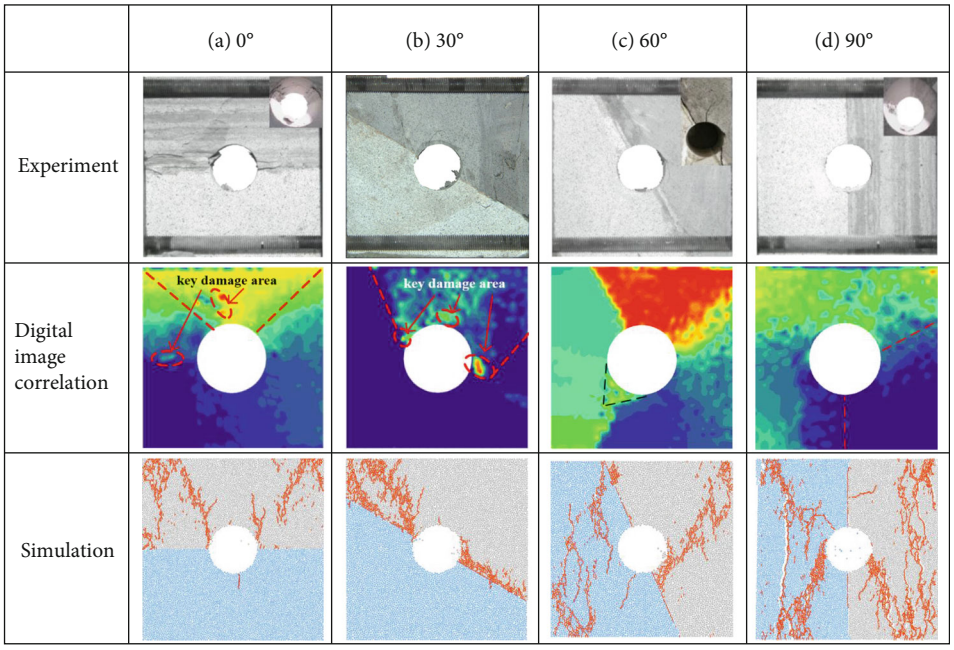


Figure 4: Comparison between simulation results and laboratory test results.

specimens with holes under different confining pressures, the biaxial compression simulation test is carried out. Figure 5 shows stress-strain curves and the number of cracks of specimens with various dip angles under different confining pressure. Taking specimen with $\alpha = 0^\circ$ as an example, with the increase of the confining pressure, the peak strength of the composite rock specimen with holes increased from 12.4 MPa to 16.6 MPa, an increase of 34%. When the dip angle of the specimen is small ($\alpha = 0^\circ$, $15^\circ$, $30^\circ$, and $45^\circ$), the stress-strain curve will fluctuate before the peak. However, for the specimens with large dip angles ($\alpha = 60^\circ$, $75^\circ$, and $90^\circ$), the stress-strain curve does not fluctuate before the peak strength. This is related to which rock area (soft or hard rock) mainly bears the axial stress when the axial load is applied. With the increase of the confining pressure, the yield stage of the stress-strain curve becomes longer, and the yield strength gradually increases, which shows that under the effect of confining pressure, deformation characteristics of specimens change from brittle failure to ductile failure.

It can be seen from the trends in Figure 5 that the number of microcracks in the specimen also shows an increasing trend with increased confining pressure. At the initial stage of loading, there is no microcrack generated. When the axial strain increased, microcracks begin to appear. When the axial strain is close to the peak strain of the specimen, the number of cracks produced by the specimen suddenly increases. This is because when the axial loading pressure

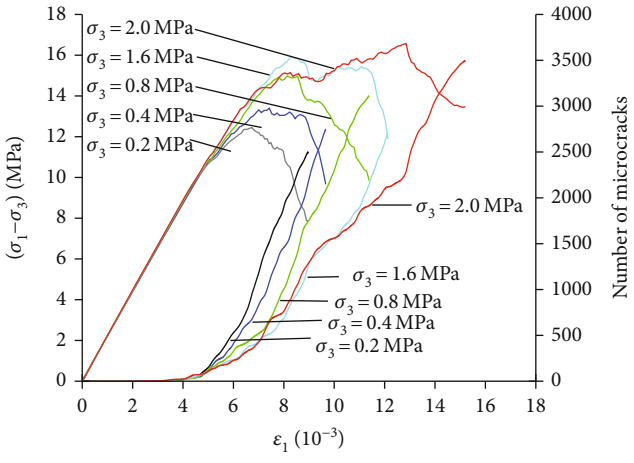


(a) $\alpha = 0°$

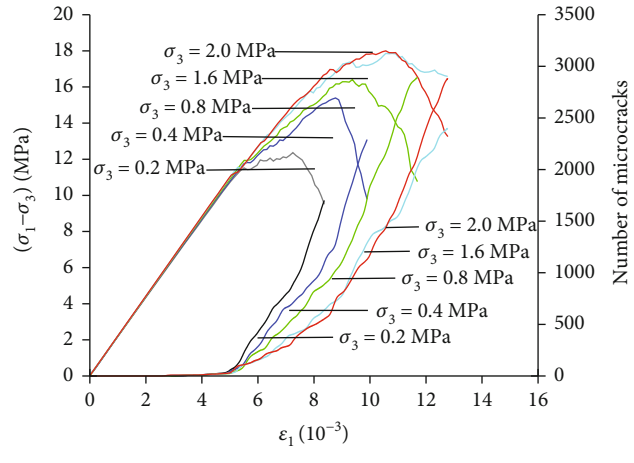


(b) $\alpha = 15°$

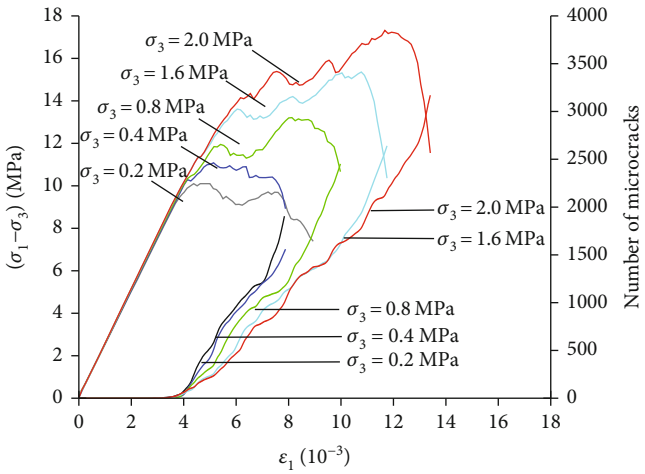


(c) $\alpha = 30°$

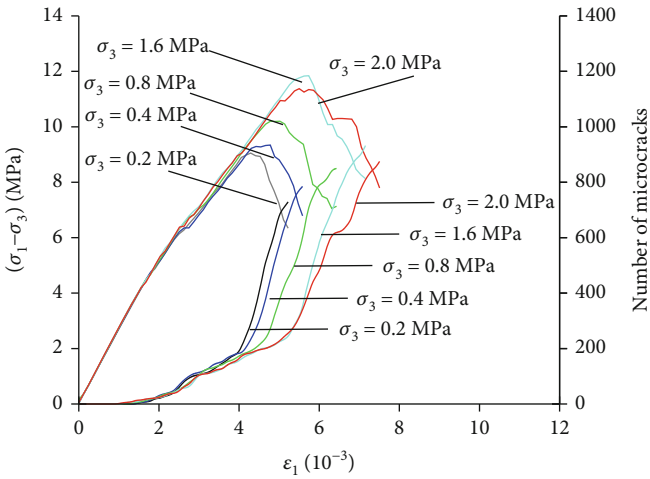


(d) $\alpha = 45°$

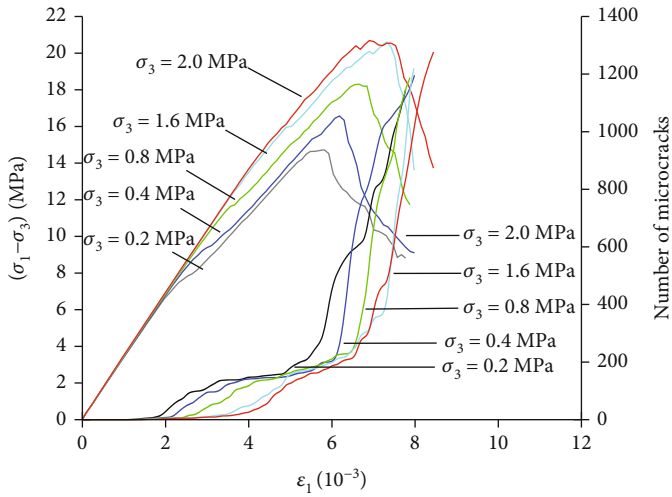


(e) $\alpha = 60°$

Figure 5: Continued.

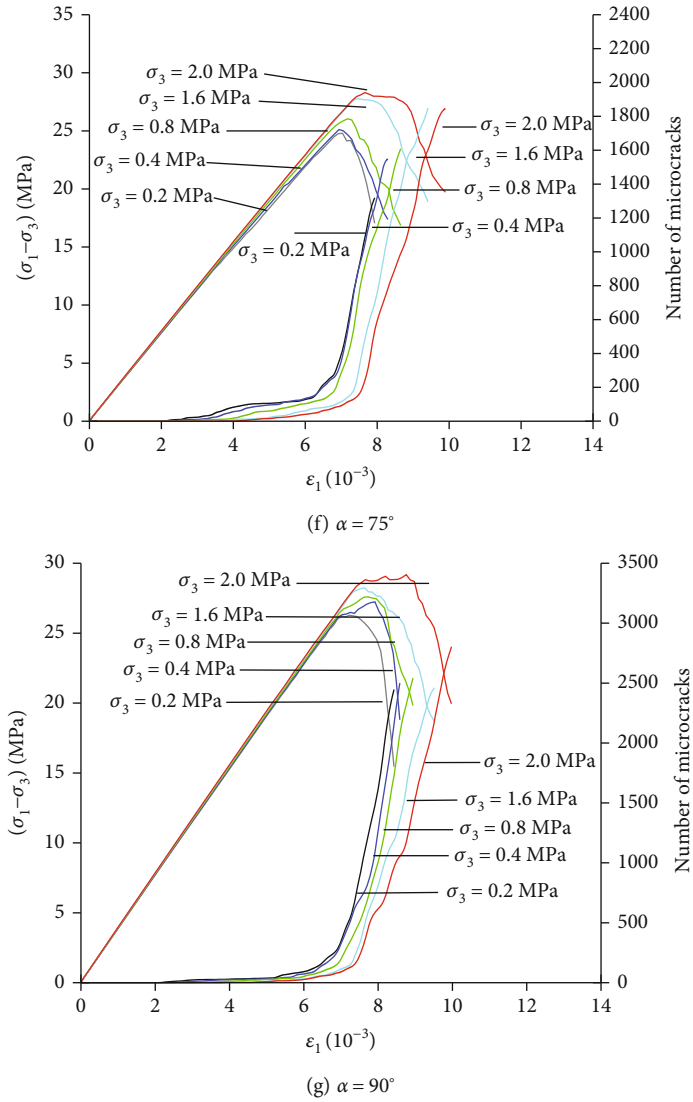


Figure 5: Stress and microcracks number versus axial strain curves under different confining pressures.

is close to the peak strength, the specimen enters the plastic stage, resulting in irreversible plastic deformation and a large number of internal cracks. When the confining pressure increases from 0.2 MPa to 2.0 MPa, the number of microscopic cracks in the specimen at the same strain is reduced. This reveals that the applied confining pressure limits the lateral deformation of the specimen, thus it is more difficult for the specimen to fail.

Figure 6 shows the variation of the compressive strength and elastic modulus with various dip angles of composite rock specimens with holes under different confining pressure. It can be seen from Figure 6(a) that the peak intensity decreases first and then increases as the dip angles increases from 0° to 90°.The minimum and maximum peak strength appear in the specimen with $\alpha = 45°$ and 90°, respectively. Figure 6(b) shows the influence of confining pressure and dip angle on the elastic modulus of the specimen. When the dip angle of the specimen increases from 0° to 90°, the elastic modulus first decreases and then gradually increases. The minimum and maximum elastic modulus appears in the specimens with a dip angle of 30° and 90°, respectively.

*4.2. Analysis of Macroscopic Failure Mode in the Biaxial Test.* Figure 7 shows the final failure mode of the composite rock specimen with holes under different dip angles and confining pressures. The red and black lines in the figure represent tensile microcracks and shear microcracks, respectively. When the dip angle of the composite rock specimen is small ($\alpha = 0°$ to 30°), the microcracks are mainly concentrated in the soft rock area and only a small number of microcracks are generated in the hard rock area. When the dip angle comes to 45°, the specimen also produces a large number of microcracks in the soft rock area and a small number of microcracks in the hard rock area. Due to the influence of the dip angle, the bond between the specimen planes is first broken, and a shear slip failure occurs along the structural plane in the specimen. For the specimens with large dip angle ($\alpha = 60°$, 75°, and 90°), a large number of microscopic

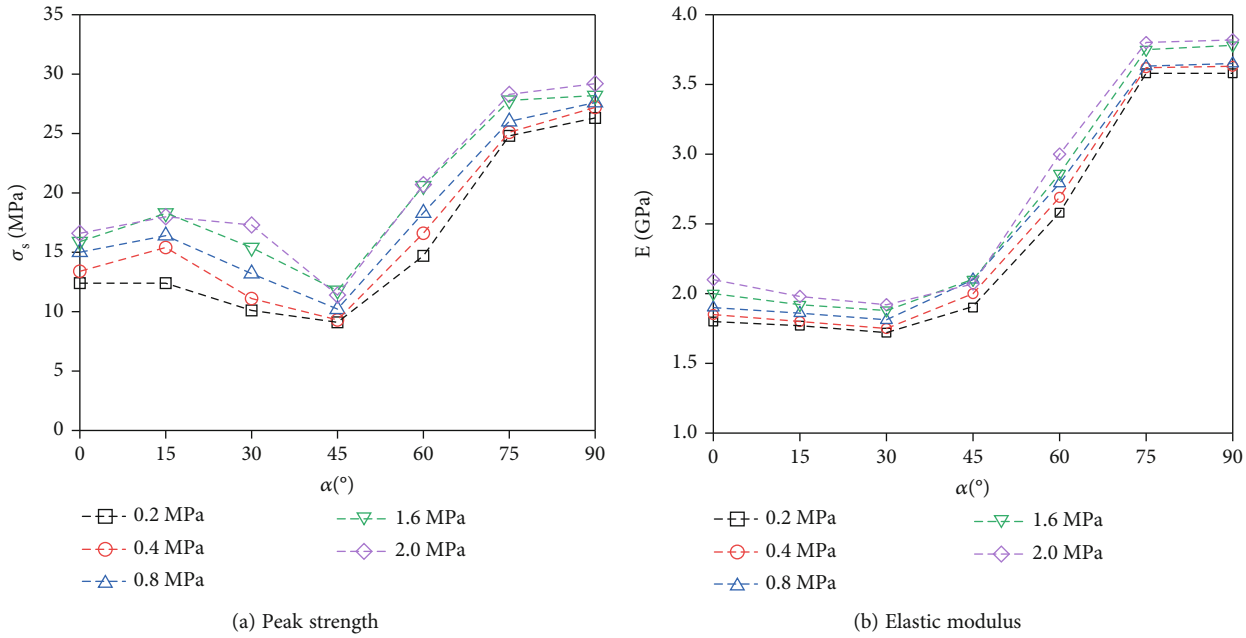


(a) Peak strength

(b) Elastic modulus

FIGURE 6: Effects of different dip angles and confining pressures on mechanical parameters of composite rock strata specimens with holes; $\sigma_s$ and $E$ stand for peak strength and elastic modulus.

cracks will be generated in the soft rock and hard rock areas. However, there are more cracks on the side of the hard rock area than that on the soft rock area, and the cracks first occur in the hard rock area. This is due to the hard rock bearing most of the axial load and having a certain supporting effect on the soft rock. Therefore, the composite rock strata with hole show an obvious asymmetric fracture mode with various dip angles, and attention needs to be paid in excavation and support design of tunnels and chambers under the condition of soft and hard alternate rock strata.

Under the effect of confining pressure, the failure modes of composite rock strata with holes are also varied. As for the specimens with a small dip angle ($\alpha = 0^\circ \sim 15^\circ$), the failure of the specimen is caused by the combined action of tensile cracks and shear cracks in low confining pressure. The V-shaped shear failure occurred in the soft rock area, and tensile failure occurred in the hard rock area. Part of the rock mass inside the hole of the composite rock specimen began to spall, and spalling mainly occurred in the soft rock area. As the confining pressure gradually increased, the failure mode did not change significantly, but the number of spalling rock mass are increasing. The phenomenon indicates that the confining pressure restricts the lateral deformation of the specimen. When the dip angle comes to medium ($\alpha = 30^\circ$ and $45^\circ$), the tensile cracks and shear cracks in the specimen gather along the dip direction of the rock structural plane, then the shear failure along the structural plane mainly occurs. For the composite rock specimen with $\alpha = 30^\circ$, tensile failure and shear failure occurs on the side of the soft rock with the increase of confining pressure. In the composite rock specimen of $\alpha = 60^\circ$ and $75^\circ$, the soft rock area and hard rock area of the specimen changed from tensile failure to shear failure with the increase of confining pressure. As the dip angle reaches $90^\circ$, the specimen shows obvious diagonal shear failure in the low confining pressure, and the specimen undergoes X-shaped shear failure under high confining pressure.

*4.3. Analysis of the Stress Field in the Biaxial Test.* Figure 8 shows the distribution of contact force around the hole in the composite rock specimens with different dip angles under different confining pressures when microcracks have not occurred. The contact force distribution diagrams at four dip angles of $0^\circ$, $30^\circ$, $60^\circ$, and $90^\circ$ are selected as examples. The gray and red lines in the figure represent compressive stress and tension stress, respectively, the thickness of the line segment represents the size of the bonding force, and the direction of the line segment represents the direction of the bonding force. It can be seen from the results that the parallel cohesive force between the particles in the specimen is constantly evolving with the change of the rock dip angle under different confining pressures.

When the confining pressure is low (0.2 MPa and 0.4 MPa), tensile stress concentration areas appear at the upper and lower parts around the hole, while compressive stress concentration areas appear on the left and right sides. As the confining pressure increases, the range of the tensile stress concentration area keeps shrinking for the specimens with small dip angles ($0^\circ$ and $30^\circ$). When the confining pressure increases to 2.0 MPa, the tensile stress concentration area is no longer obvious and the range of the compressive stress concentration area changes less. Therefore, tensile cracks are not easy to appear on the upper and lower sides of the hole under high confining pressure. As for the specimen with large dip angles ($60^\circ$ and $90^\circ$), the tensile stress concentration area on the upper and lower sides of the hole gradually shrinks until it disappears along the dip direction with the confining pressure increases. The compressive

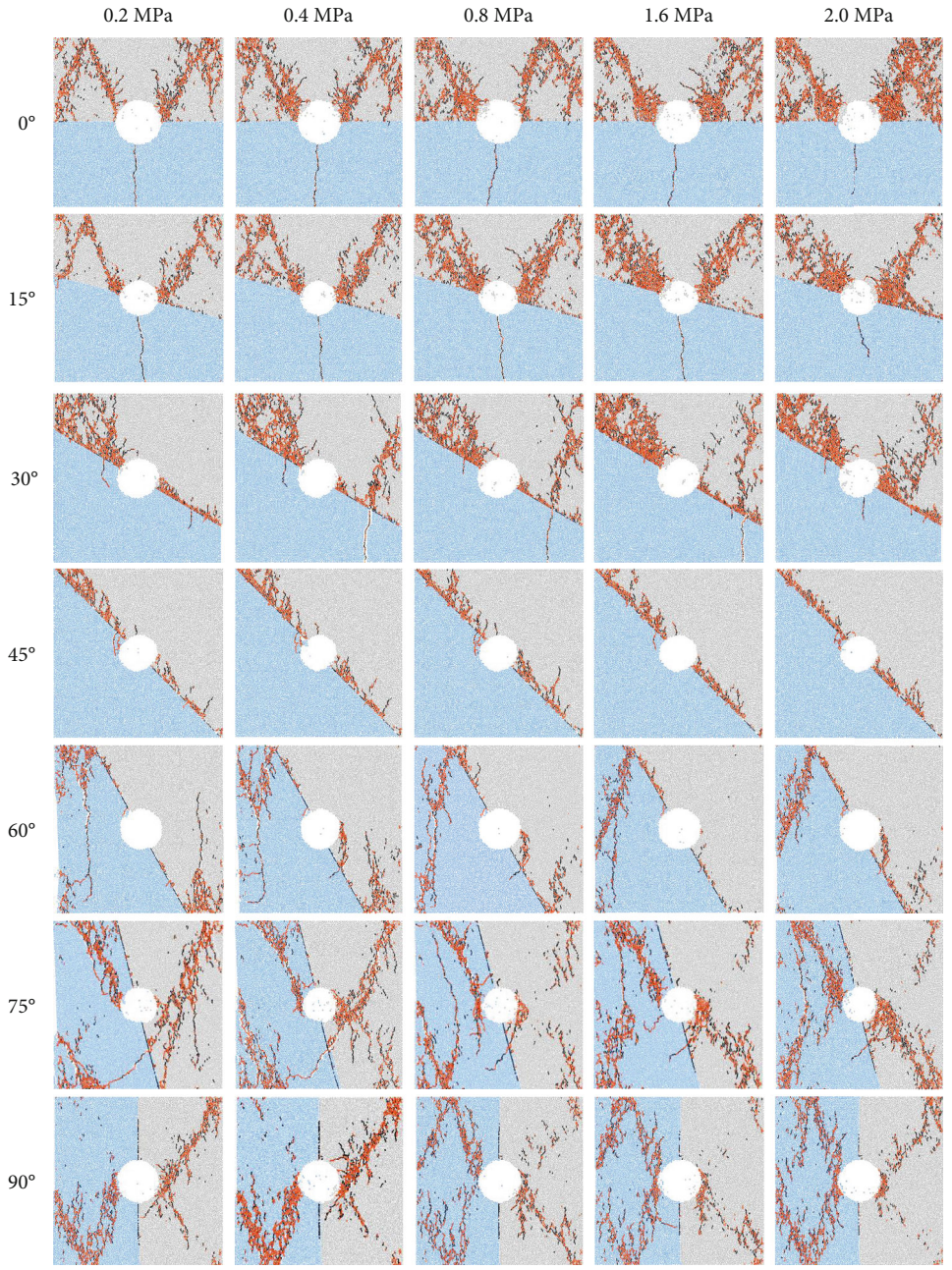


Figure 7: Failure mode of composite rock strata specimen with holes under different confining pressures and different dip angles.

stress concentration area in the direction of perpendicular to the rock strata dip increases on the hard rock side, and there is no obvious change in the extent of the tensile stress concentration area on the soft rock side. In the case of the same confining pressure, the tensile stress concentration area shifts to the hard rock part as the dip angle of the specimen increases. The range of compression stress concentration area in the hard rock strata is larger than that in the soft rock side which shows an asymmetry distribution. Therefore, tensile cracks will first appear on the upper and lower sides of the composite specimen when the confining pressure is low. As the confining pressure increases, the tensile stress concentration area gradually transfers and disappears, and the compressive stress concentration areas on the left and right sides of the specimen will lead to crack generation.

The continuous changes of the tensile stress and shear stress concentration areas in the composite specimen are accompanied by the generation of microcracks. The difference in generation, expansion, and coalescence of microcracks leads to changes in the macroscopic failure model of the specimen. Therefore, based on the analysis of the evolution process of the contact force between particles, the failure laws of composite rock specimens with different dip angles under different confining pressures can be revealed.

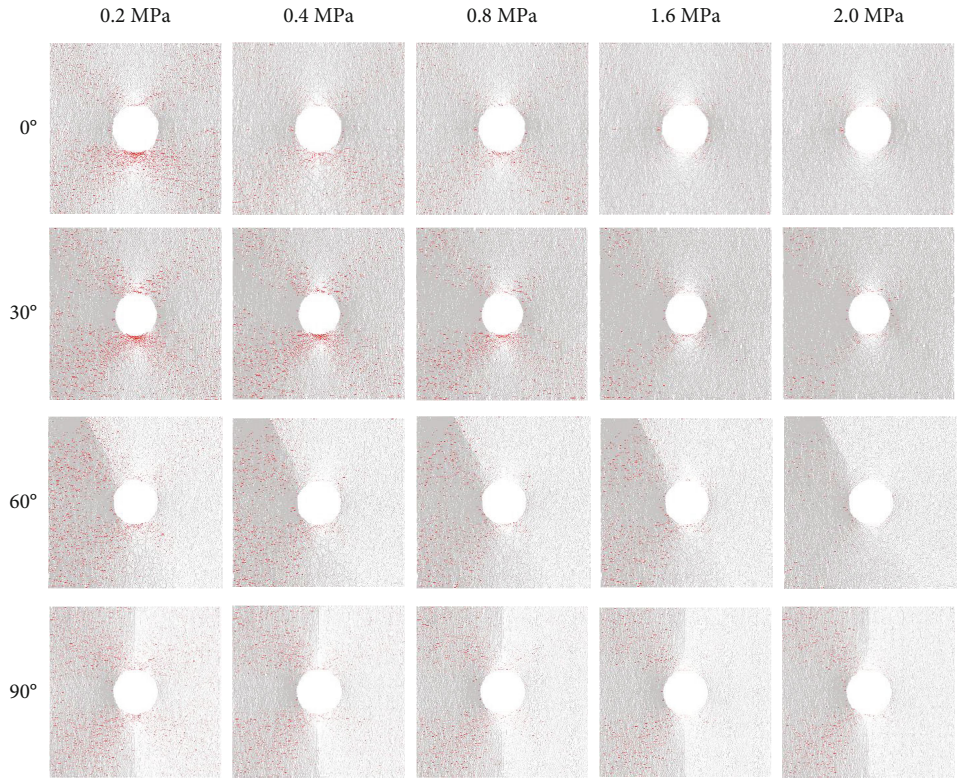


Figure 8: Distribution of contact force around the hole before crack initiation under different confining pressures.

*4.4. Displacement Field Analysis.* Taking the particle displacement vector distribution of the rock specimens with holes at a dip angle of 60° for example, the influence of confining pressure on the cracking characteristics analyzed, as shown in Figure 9. The arrow in the figure represents the displacement direction of the particles, and the length of the arrow line segment represents the magnitude of the displacement. To describe the movement trend of the particles around the crack more vividly, the blue solid arrow in the right larger version is used to describe the displacement direction of the particles. According to the relative displacement vector direction and size of adjacent particles on both sides of the crack, this study simplified and classified the relative displacement between particles. Based on the previous research results [32],the failure modes can be divided into five simplified types according to the final relative displacement field form, namely direct tensile and relative tensile(RT), direct shear(DS), relative shear(RS) and mixed failure(MF) modes.

Figure 9(a) shows the displacement field vector diagram of the specimen with $\alpha = 60^{\circ}$ under the confining pressure of 0.2 MPa. The particles on both sides of the crack at position 1 of the specimen showed RT tensile failure. The particles at position 2 move in different directions and finally present the MF-2 mixed failure mode. The displacement of the particles at position 3 on the left side of the crack is smaller than that on the right side, and eventually, DS-1 direct shear failure occurs. The particles on the sides of the crack move in the same direction with different displacements, and the specimen undergoes RT-type tensile failure at position 4 below the hole. When the confining pressure comes to 0.4 MPa and 0.8 MPa, the displacement field distribution of the specimen is shown in Figures 9(b) and 9(c). The displacement field distribution diagram of each position when the specimen is broken has little change compared with the case of 0.2 MPa. The particles at position 2 at the upper left of the hole still undergo mixed failure, but the failure mode has changed from MF-2 mixed failure to MF-1 mixed failure. As the confining pressure continues to increase, the displacement field vector diagram of the specimen at 1.6 MPa is shown in Figure 9(d). At this time, the failure mode at position 2 on the left side of the hole changes from MF-1 mixed failure to DS-1 shear failure. There is no significant change in failure mode at locations 1, 3 and 4.As the confining pressure increases to 2.0 MPa (Figure 9(e)), the microcracks at position 1 at the lower left of the hole disappear, and DS-1 shear failure still occurs at position 2. The failure mode of position 3 above the hole and position 4 below the right of the hole has not changed significantly.

By analyzing the displacement field of the composite rock specimen with holes at a dip angle of 60° under different confining pressures, it can be concluded that the displacement field at different positions of the specimen shows different changing laws. As the confining pressure increases from 0.2 MPa to 1.6 MPa, RT tensile failure occurs at position 1 on the left side of the hole. When the confining pressure increases to 2.0 MPa, the tensile crack disappears and no macro fracture zone is generated, this shows that the tensile failure at position 1 is suppressed. With the increase of the confining pressure, the failure mode at the upper left position 2 of the specimen also changed significantly. The failure mode at this position changed from the

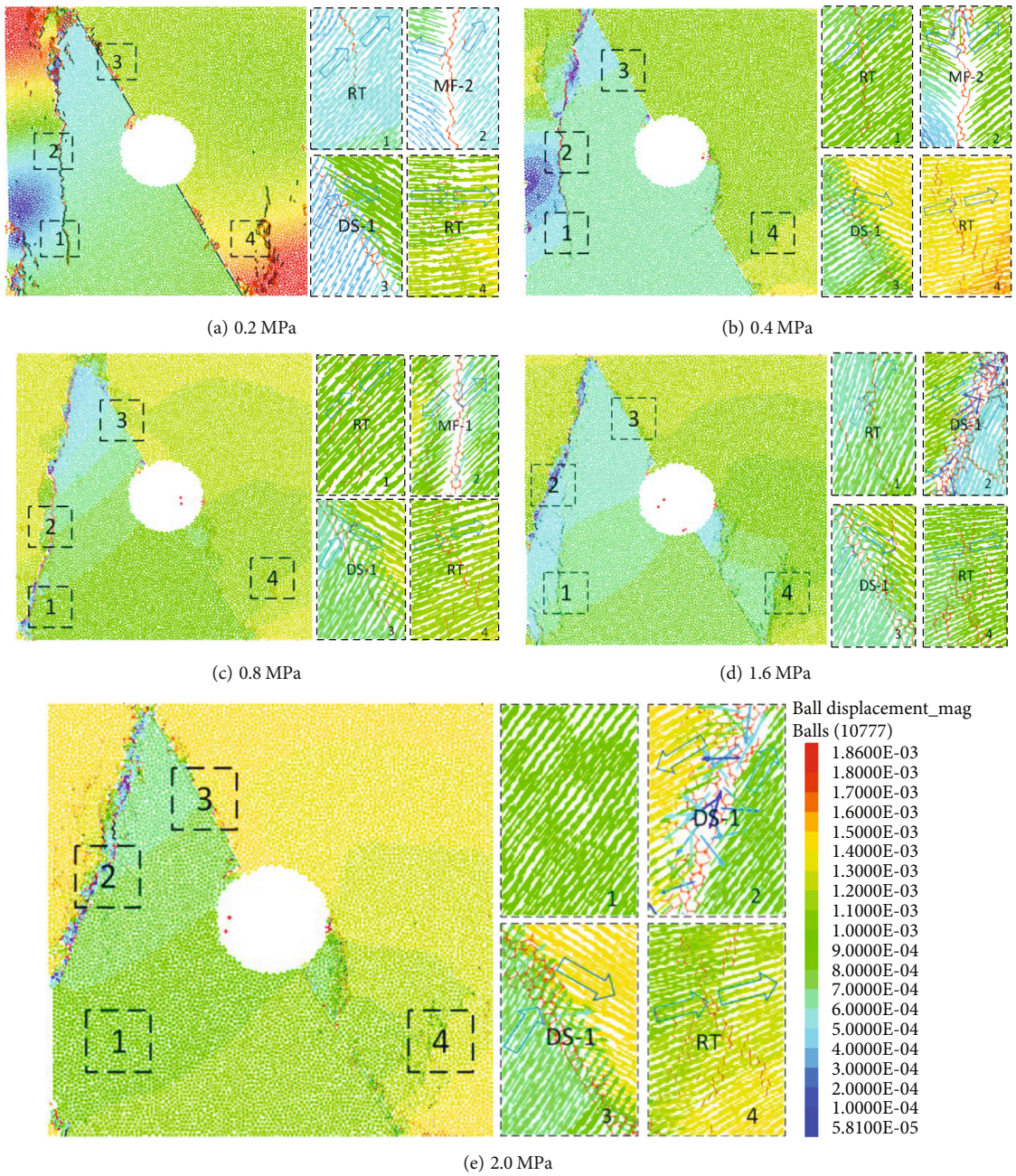


(a) 0.2 MPa (b) 0.4 MPa

(c) 0.8 MPa (d) 1.6 MPa

(e) 2.0 MPa

Figure 9: Displacement field vector diagram of 60° composite rock specimen under different confining pressures.

mixed failure of MF-2 and MF-1 to the shear failure of DS-1. This indicates that the tensile failure zone in the hard rock strata is transformed into a shear failure zone.

## 5. Conclusion

(1) The mechanical behavior of specimens containing the hole is significantly influenced by dip angle and confining pressure. As the dip angle of the rock strata increases, the peak strength and elastic modulus show a trend of first decreasing and then increasing, both of which achieve the maximum value at 90°. The peak strength achieves the minimum value when the dip angle is 45°, and with a minimum value at 30° for elastic modulus. As the dip angle is constant, with the confining pressure increases both the peak strength and elastic modulus gradually increase

(2) The macroscopic failure mode of the specimen is affected by the confining pressure and the dip angle. At low dip angles ($\alpha = 0°\sim15°$), soft rock strata often fail first, and the increase in confining pressure has little effect on the failure mode. For the specimens with medium dip angles ($\alpha = 30°\sim45°$), the fracture mode is controlled by the structural plane, and shear-slip failure occurs along the structural plane. As the confining pressure increases, the degree of

specimen fragmentation gradually deepens. For the specimens with large dip angles ($\alpha^\circ = 60^\circ \sim 90^\circ$), because the hard rock bears the main axial load, the hard rock area is more prone to failure. As the confining pressure increases, the shear failure gradually increases

(3) The distribution characteristics of the contact force around the hole are as follows: When the confining pressure is the same, as the dip angle increases, the tensile stress concentration area shifts to the hard rock side. The compressive stress concentration area in the hard rock strata is larger than the soft rock side, and the distribution of the compression stress concentration area on the left and right sides of the hole appears asymmetry. With the increase of the confining pressure, the range of the tensile stress concentration area is greatly reduced, while the range of the compressive stress concentration area changes less

(4) The displacement field analysis shows that the confining pressure has a direct effect on the failure mode of the specimen. With the increase of the confining pressure, the tensile failure in the specimen is suppressed, and the macroscopic failure zone changes from tensile failure to shear failure

## Data Availability

The data used to support the findings of this study are included within the article.

## Conflicts of Interest

The authors declare that there are no conflicts of interest.

## Acknowledgments

This research was supported by the Natural Science Foundation of Shandong Province (ZR2019MEE022, ZR2020QE119) and the National Natural Science Foundation of China (52004145).

## References

[1] G. Barla, "Full-face excavation of large tunnels in difficult conditions," *Journal of Rock Mechanics and Geotechnical Engineering*, vol. 8, no. 3, pp. 294–303, 2016.

[2] M. K. Panda, S. Mohanty, and B. M. P. Pingua, "Engineering geological and geotechnical investigations along the head race tunnel in Teesta Stage-III hydroelectric project, India," *Engineering Geology*, vol. 181, pp. 297–308, 2014.

[3] Y.-H. Li, X.-J. Tang, S. Yang, and J.-W. Chen, "Evolution of the broken rock zone in the mixed ground tunnel based on the DSCM," *Tunnelling and Underground Space Technology*, vol. 84, pp. 248–258, 2019.

[4] Q.-Y. Zhang, M.-Y. Ren, and K. Duan, "Geo-mechanical model test on the collaborative bearing effect of rock-support system for deep tunnel in complicated rock strata," *Tunnelling and Underground Space Technology*, vol. 91, p. 103001, 2019.

[5] F. Huang, H.-H. Zhu, Q.-W. Xu, Y.-C. Cai, and X.-Y. Zhuang, "The effect of weak interlayer on the failure pattern of rock mass around tunnel - scaled model tests and numerical analysis," *Tunnelling and Underground Space Technology*, vol. 35, pp. 207–218, 2013.

[6] K. Wu, Z. Shao, M. Sharifzadeh, Z. Chu, and S. Qin, "Analytical approach to estimating the influence of shotcrete hardening property on tunnel response," *Journal of Engineering Mechanics*, vol. 148, no. 1, 2022.

[7] K. Wu, Z. Shao, S. Qin, W. Wei, and Z. Chu, "A critical review on the performance of yielding supports in squeezing tunnels," *Tunnelling and Underground Space Technology*, vol. 115, p. 103815, 2021.

[8] P. Lin, H.-Y. Liu, and W.-Y. Zhou, "Experimental study on failure behaviour of deep tunnels under high in-situ stresses," *Tunnelling and Underground Space Technology*, vol. 46, pp. 28–45, 2015.

[9] X. Liu, S. Yang, Y. Huang, and J. Cheng, "Experimental study on the strength and fracture mechanism of sandstone containing elliptical holes and fissures under uniaxial compression," *Engineering Fracture Mechanics*, vol. 205, pp. 205–217, 2019.

[10] K. Wu, Z. Shao, S. Qin, N. Zhao, and Z. Chu, "An improved non-linear creep model for rock applied to tunnel displacement prediction," *International Journal of Applied Mechanics*, vol. 13, 2021.

[11] X.-F. Si, F.-Q. Gong, and L. X.-B. LuoY, "Experimental simulation on rockburst process of deep three-dimensional circular cavern, China," *Rock Soil Mechanics.vol.*, vol. 39, pp. 621–634, 2018.

[12] H. Zhou, F. Meng, C. Zhang, J. Lu, and R. Xu, "Effect of structural plane on rockburst in deep hard rock tunnels," *China, Rock MechanicsEngineering*, vol. 34, pp. 720–727, 2015.

[13] H. Wu, G. Zhao, L. W. KulatilakePhsw, and E. Wang, "Fracturing behaviour of sandstone specimens with a cavity formed by intersecting excavations under compression: experimental study and numerical modelling," *Strain*, vol. 55, no. 4, 2019.

[14] A. K. Maji and S. P. Shah, "Application of acoustic emission and laser holography to study microfracture in concrete," *NDT & E International*, vol. 112, pp. 83–110, 1989.

[15] M.-r. Du, H.-w. Jing, H.-j. Su, T.-t. Zhu, and M.-l. Chen, "Strength and failure characteristics of sandstone containing two circular holes filled with two types of inclusions under uniaxial compression," *Journal of Central South University (In Chinese)*, vol. 24, no. 11, pp. 2487–2495, 2017.

[16] A. Fakhimi, F. Carvalho, T. Ishida, and J. F. Labuz, "Simulation of failure around a circular opening in rock," *International Journal of Rock Mechanics and Mining Sciences*, vol. 39, no. 4, pp. 507–515, 2002.

[17] M. Sagong and D. Park, "Experimental and numerical analyses of an opening in a jointed rock mass under biaxial compression," *International Journal of Rock Mechanicsand Mining Sciences*, vol. 48, no. 7, pp. 1055–1067, 2011.

[18] J.-L. Cheng, S.-Q. Yang, K. Chen, D. Ma, F.-Y. Li, and L.-M. Wang, "Uniaxial experimental study of the acoustic emission and deformation behavior of composite rock based on 3D digital image correlation (DIC)," *Acta Mechanica Sinica*, vol. 33, no. 6, pp. 999–1021, 2017.

[19] H.-F. Deng, W. Wang, and J.-L. Li, "Experimental study on anisotropic characteristics of bedded sandstone," *Chinese*

*Journal of Rock Mechanics and Engineering*, vol. 37, no. 1, pp. 112–120, 2018.

[20] W. Feng, R. Huang, and T. Li, "Deformation analysis of a soft-hard rock contact zone surrounding a tunnel," *Tunnelling and Underground Space Technology*, vol. 32, pp. 190–197, 2012.

[21] S.-Q. Yang, M. Chen, and G. Fang, "Physical experiment and numerical modelling of tunnel excavation in slanted upper-soft and lower-hard strata," *Tunnelling and Underground Space Technology*, vol. 82, pp. 248–264, 2018.

[22] X. Wang, Z. Xia, P. Li, and H. Liu, "Numerical study on strength and failure behavior of rock with composite defects under uniaxial compression," *Energies*, vol. 14, no. 15, p. 4418, 2021.

[23] W. C. Zhu, J. Liu, C. A. Tang, X. D. Zhao, and B. H. Brady, "Simulation of progressive fracturing processes around underground excavations under biaxial compression," *Tunnellingand Underground Space Technology*, vol. 20, no. 3, pp. 231–247, 2005.

[24] P. Hou, X. Liang, F. Gao, J.-B. Dong, J. He, and Y. Xue, "Quantitative visualization and characteristics of gas flow in 3D pore-fracture system of tight rock based on lattice Boltzmann simulation," *Journal of Natural Gas Science and Engineering*, vol. 89, no. 4, p. 103867, 2021.

[25] P. Hou, X. Liang, Y. Zhang, J. He, F. Gao, and J. Liu, "3D multi-scale reconstruction of fractured shale and influence of fracture morphology on shale gas flow," *Natural Resources Research*, vol. 30, no. 3, pp. 2463–2481, 2021.

[26] X. Liang, P. Hou, Y. Xue, X.-J. Yang, F. Gao, and J. Liu, "A fractal perspective on fracture initiation and propagation of reservoir rocks under water and nitrogen fracturing," *Patterns and Scaling in nature and Society*, vol. 29, no. 7, 2021.

[27] G.-C. Zhang, C.-W. Zang, M. Chen, G. Tao, and D. Zhao, "Ground response of entries driven adjacent to a retreating longwall panel," *International Journal of Rock Mechanics and Mining Sciences*, vol. 138, p. 104630, 2021.

[28] S. Yang, Y.-H. Li, M. Chen, and J.-S. Liu, "Incompatible deformation and damage evolution of mixed strata specimens containing a circular hole," *Geomechanics and Engineering*, vol. 20, no. 5, pp. 461–474, 2020.

[29] S.-Q. Yang, P.-F. Yin, Y.-C. Zhang et al., "Failure behavior and crack evolution mechanism of a non-persistent jointed rock mass containing a circular hole," *International Journal of Rock Mechanics and Mining Sciences*, vol. 114, pp. 101–121, 2019.

[30] Itasca, *Users Manual for Particle Flow Code in 2 Dimensions (PFC2D), Version 3.1*, Minneapolis: Itasca Consulting Group, Inc, 2002.

[31] D. O. Potyondy and P. A. Cundall, "A bonded-particle model for rock," *International Journal of Rock Mechanics and Mining Sciences*, vol. 41, no. 8, pp. 1329–1364, 2004.

[32] M. Chen, S.-Q. Yang, P. G. Ranjith, and Y.-C. Zhang, "Cracking behavior of rock containing non-persistent joints with various joints inclinations," *Theoretical and Applied Fracture Mechanics*, vol. 109, p. 102701, 2020.